

Ecological sustainability assessment for  
Firth of Thames shellfish aquaculture:  
Task 1 - Hydrodynamic Modelling

July 2003 EW TR 05/05 ARC TP 252







Ecological sustainability assessment  
for Firth of Thames shellfish  
aquaculture:  
Task 1 - Hydrodynamic Modelling

July 2003

Environment Waikato Technical Report number 05/05  
Auckland Regional Council Technical Publication number TP 252

Auckland Regional Council  
Technical Publication No. 252, July 2003  
Environment Waikato Technical report 05/05  
ISSN 1175 205X ISBN 1-877353-67-1

Printed on recycled paper



---

# Ecological sustainability assessment for Firth of Thames shellfish aquaculture: Task 1 – Hydrodynamic modelling

---

Scott Stephens

**Prepared for**  
Auckland Regional Council  
Environment Waikato  
Western Firth Consortium

NIWA Client Report: HAM2003-113  
July 2003

NIWA Project: ARC03292

National Institute of Water & Atmospheric Research Ltd  
Gate 10, Silverdale Road, Hamilton  
P O Box 11115, Hamilton, New Zealand  
Phone +64-7-856 7026, Fax +64-7-856 0151  
[www.niwa.co.nz](http://www.niwa.co.nz)



# Contents

---

Executive Summary	iv
1. Introduction and scope of work	2
1.1 Introduction	2
2. Modelling approach	4
2.1 Hydrodynamic model	4
2.2 Model set-up	4
2.2.1 Bathymetry	4
2.2.2 Vertical grid structure	6
2.2.3 Turbulence closure	6
2.2.4 Temperature and salinity dispersion	7
2.2.5 Seabed resistance	7
2.3 Forcing inputs to the model	7
2.3.1 Tide	7
2.3.2 Stratification	8
2.3.3 Temperature	9
2.3.4 Salinity	9
2.3.5 Wind	9
2.3.6 "Worst-case" winds	10
2.3.7 Rivers	13
2.3.8 Heat exchange	13
2.3.9 Relative Humidity	14
2.3.10 Model output	14
3. Model calibration	16
3.1 Tides	16
3.2 Temperature calibration	17
3.3 Residual currents	20
4. Results – Firth of Thames hydrodynamics	22
4.1 Tidal currents	22
4.2 Wind-driven currents	24
4.3 "Worst-case" winds	27
5. Conclusions	30
6. References	32
7. Glossary	34

---



# Executive Summary

The Auckland Regional Council, Environment Waikato and Western Firth Consortium contracted NIWA to undertake an ecological sustainability assessment for aquaculture in the Firth of Thames. This report addresses task 1 of 4; hydrodynamic modelling of the Firth of Thames to produce a series of spatially resolved timeseries of velocity vectors, temperature and salinity as inputs to subsequent tasks.

The three-dimensional numerical model MIKE3 was used to simulate hydrodynamics in the Firth of Thames. The model included both temperature and salinity, and was forced by tides, winds, solar radiation and river inputs. Data was output at ½-hour intervals for use in subsequent tasks.

The model was calibrated against available environmental data measured during September 1999 and March 2000, during a La Nina period. No environmental data was available to calibrate for El Nino conditions.

The long-term wind record from the Mokohinau Islands was examined for El Nino, La Nina, summer and winter trends. It was observed that the seasonal signal masked the SOI signal, so a 1-month simulation could not adequately represent SOI trends. Therefore, month-long wind records from the Mokohinau Islands were selected to represent “worst-case” wind scenarios, when the wind approached from either the NE–N or SW–W sectors for more than 50% of the time. For each sector, the selected periods were then ranked on their closeness of fit to a wind speed criterion, the mean NE–E wind speed should be 2 standard-deviations above the long-term NE–E mean, while the SW–W speed should be 2 standard-deviations below, and vice versa. The period 21 Feb to 23 March 1962 was chosen to represent winds prevailing from the ENE, and the period 30 June to 30 July 1976 to represent winds prevailing from the WSW. Another four simulations were undertaken combining each “worst-case” wind scenario with both the summer and early spring calibration data.

Tides dominated the instantaneous flow field in the Firth of Thames, with strongest flows in the outer Firth reaching 0.2 and 0.4 m s<sup>-1</sup> during neap and spring tides respectively. Tidal flows were less than 0.05 m s<sup>-1</sup> in the shallow southern Firth. Flood tides were deflected upward around Deadmans Point near Kirita Bay, causing time-averaged upwelling in its vicinity. The Earth’s rotation deflects currents to the left, causing flood tides to be stronger on the eastern side of the Firth near Wilsons Bay and ebb tides to be stronger on the western side.

Wind was of secondary importance to the instantaneous currents, but had a dominant influence on time-averaged currents, which show cumulative flow features. When winds approached from the ENE, surface currents were pushed southwest with a time-averaged clockwise circulation in the lower Firth, and deep currents returned toward the north. When winds approach from the WSW, surface currents were pushed northeast with a time-averaged anticlockwise circulation in the lower Firth, and deep currents returned toward the southwest. The affect of stratification in de-coupling vertical water “layers” means that particles near the water surface are likely to remain there and be transported faster by wind-driven flows during summer than in winter.



# 1. Introduction and scope of work

## 1.1 Introduction

The Auckland Regional Council, Environment Waikato and Western Firth Consortium contracted NIWA to undertake an ecological sustainability assessment for aquaculture in the Firth of Thames. The contract consists of four tasks. This report addresses task 1; hydrodynamic modelling of the Firth of Thames to produce a series of spatially resolved timeseries of velocity vectors, temperature and salinity as inputs to subsequent tasks. Circulation patterns obtained from this task will be used to determine biologically important characteristics such as the flushing time and routes by which water and materials are transported through the Firth of Thames and Hauraki Gulf.

The numerical model and modelling approach are described first. Environmental data used to drive the model is then presented; including an analysis of the long-term Mokohinau Islands wind record. Calibration results are followed by a general description of hydrodynamics in the Firth of Thames.



## 2. Modelling approach

### 2.1 Hydrodynamic model

The hydrodynamic model used in this study was the DHI Water and Environment three-dimensional model MIKE3, an engineering software package containing a comprehensive modelling system for 3D free-surface flows. MIKE3 is applicable to the simulation of hydraulic and related phenomena in coastal areas and seas where stratification or vertical circulation is important. The hydrodynamics are solved on a fixed grid of square cells using the mass conservation equation, the Reynolds-averaged Navier-Stokes equations, including the effects of turbulence and variable density, and the conservation equations for salinity and temperature in three dimensions together with the equation of state of sea water relating the local density to salinity, temperature and pressure.

### 2.2 Model set-up

#### 2.2.1 Bathymetry

The most important input to any hydrodynamic model is the bathymetry. For this study two bathymetry grids were required. The first covered the entire Hauraki Gulf and was used to check tidal calibration (Figure 1), while the second covered the Firth of Thames area (Figure 2) and was used for the bulk of the numerical simulations. The Hauraki Gulf grid was originally developed during a NIWA research programme “Nearshore-Offshore Exchange”, funded by the Foundation for Research, Science and Technology (Black et al. 2000). The Hauraki Gulf grid consists of a regular grid of 130×210 cells, each 750 m square, the grid orientated North/South with its origin at 2,640,000 m (E), 6,437,500 m (N) in terms of NZMG (Figure 1).

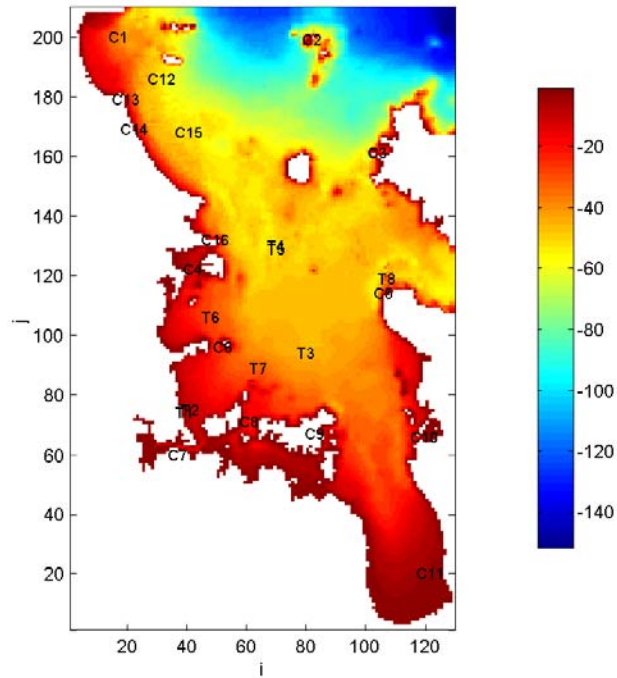


**Figure 1:** The 750 m-square Hauraki Gulf model grid, with tidal calibration sites marked ( Table 1, Table 2). Colour scale indicates depth (m).

The Firth of Thames grid is a subset of the Hauraki Gulf grid, incorporating 750 m cells 20-130 in the east-west direction and cells 1-114 in the north-south direction. Wet cells on the eastern side of Coromandel peninsula were blocked out since they were irrelevant to the Firth of Thames simulations (Figure 2).

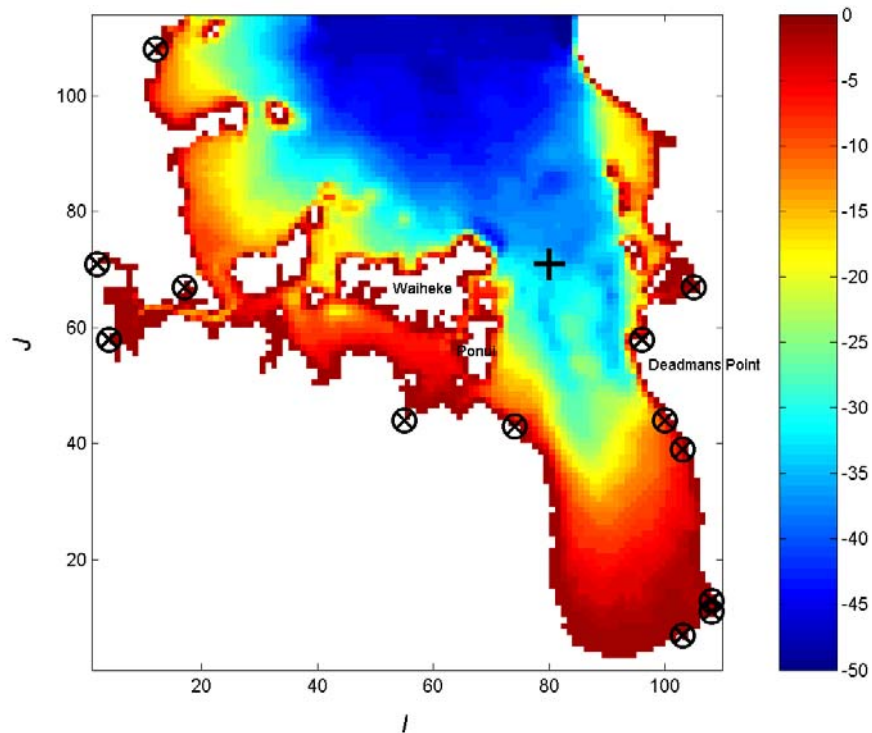


**Figure 2:** Firth of Thames 750 m bathymetry grid. Colour scale indicates depth (m). River sources are marked ⊗. The FoT mooring site is marked +.

### 2.2.2 Vertical grid structure

For the Firth of Thames simulations the model used  $20 \times 2$  m-thick vertical layers. The centre of the uppermost layer is 2 m below datum, and the centre of each subsequent layer is 2 m below that. The uppermost layer is therefore 3 m thick, while others are 2 m thick. Water level oscillations, such as tides, cause variations in the thickness of the surface layer. For depths greater than 40 m, the lowermost cell grows to reach the seabed, and for shallower depths layers drop out from the bottom up, with the lowermost layer always greater than 1 m thick.

### 2.2.3 Turbulence closure

The mixed  $k$ - $\varepsilon$ /Smagorinsky formulation was employed for this study, using the default parameters. This scheme uses the Smagorinsky formulation in the horizontal and a standard 1-dimensional  $k$ - $\varepsilon$  model in the vertical. This uses transport equations for two quantities to describe the turbulent motion: the turbulent kinetic energy,  $k$ , and the dissipation rate of turbulent kinetic energy,  $\varepsilon$ . Advantages of the mixed scheme are that the  $k$ - $\varepsilon$  model has well-trialled coefficients that require less calibration, and buoyancy effects are accounted for.

## 2.2.4 Temperature and salinity dispersion

The dispersion of salinity and temperature is assumed to be proportional to the effective Eddy Viscosity with the factor of proportionality being  $1/\sigma_T$ , the dispersion factor.  $\sigma_T$  is the Prandtl/Schmidt number. Values of  $\sigma_T$  greater than one imply that diffusive transport is weaker for salt/temperature than for momentum. Dispersion factors of 0.1 and 0.01 were used in the horizontal and vertical directions respectively to account for weaker vertical mixing due to stratification.

## 2.2.5 Seabed resistance

The default parameter was used. The model is largely insensitive to the bottom friction coefficient in the water depths experienced in most of the Firth of Thames. The region most affected by seabed friction is the shallow southern Firth, where seabed friction will retard the tidal flow. This region is not a critical area for the study.

## 2.3 Forcing inputs to the model

### 2.3.1 Tide

Tidal water level variations were applied to the open-sea boundaries of the model grids (Figure 3). Both spring and neap tides were represented during the calibration simulations.

For the Firth of Thames model (Figure 2), tides were forced at the open boundary using the 13 most dominant tidal constituents  $M_2$ ,  $S_2$ ,  $N_2$ ,  $K_2$ ,  $K_1$ ,  $O_1$ ,  $P_1$ ,  $Q_1$ ,  $2N_2$ ,  $MU_2$ ,  $NU_2$ ,  $L_2$  and  $T_2$ . This was done by extracting the phase and amplitude of each of the tidal constituents from the larger EEZ model (Goring, 2001) at the positions of each of the offshore ocean boundary cells located along the north side of Figure 2.

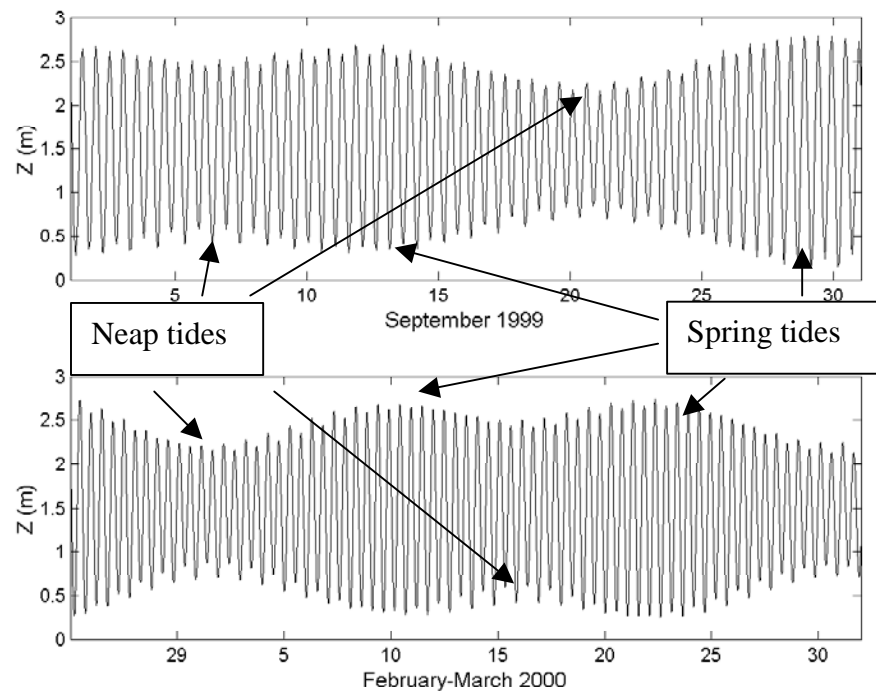


**Figure 3:** Sea-surface heights (m above Moturiki datum) prescribed at the models seaward boundary for September 1999 and March 2000 simulations. Mean sea level is 1.487 m above Moturiki datum.

### 2.3.2 Stratification

Stratification occurs when light buoyant water overlies heavy dense water. Stratification is caused either by temperature differences: warm water is lighter than cold water, or by salinity differences: freshwater is lighter than seawater. In winter the Firth of Thames becomes stratified by freshwater runoff from the surrounding catchments, while in summer it becomes temperature stratified as well, by solar radiation and heat exchange with warm air. The summer temperature stratification is generally much stronger than freshwater stratification during winter, although the effect of large floods is unknown.

Stratification does not affect tidal flows much, but the water column response to wind-driven currents can be highly modified by stratification.

The buoyancy force resists vertical change, so a water 'parcel' will tend not to move vertically when the water column is stratified. Therefore, it is much easier for currents to flow horizontally than vertically when the water is stratified. For example, wind-driven surface currents will tend to flow horizontally above the thermocline, and where these currents run into the coast, bottom-return-flows can form flowing in the reverse direction below the thermocline.

Conversely, in unstratified or homogeneous water, there tends to be more horizontal variability and flows are more vertically uniform, as momentum becomes more evenly distributed throughout the water column. Eddies and current jets are more likely to form as

wind-driven currents become deflected by the topography. This can lead to complex circulation patterns.

### 2.3.3 Temperature

Aside from solar radiation inputs at the water surface the model requires an initial temperature field to be set, and thereafter requires water temperatures to be input at the open boundary at each timestep. Obtaining accurate internal temperature fields is a challenging task because of naturally high spatial variability created by subtleties such as cloud cover. Furthermore, it is practically impossible to measure temperature everywhere on the open boundary to use as input, and initial conditions are often guessed for the same reasons.

Sea surface temperature data were unavailable for the calibration period, so water temperature inputs to the model were derived from measurements taken at two sites, a thermistor chain located in the Firth of Thames (Figure 2) and one located on the continental shelf edge offshore from Whangarei. Temperature fields were interpolated vertically using linear interpolation and horizontally using a cubic inverse-distance function. Both initial temperature fields and boundary timeseries were created like this. Obviously there are considerable uncertainties associated with interpolating over a large area using such a paucity of data. Fortunately the model boundary was located far enough north that temperatures did not advect into the Firth of Thames on the flood tide, leaving the local temperature field to evolve mainly due to solar and riverine inputs. I am therefore confident that the calibrations are largely unaffected by the temperature boundary condition.

River temperatures were specified as 11°C during winter and 22°C during summer.

### 2.3.4 Salinity

The background salinity was set to 35.3 psu. River salinities were set to 4 psu.

### 2.3.5 Wind

To force the calibrated model simulations, wind data were obtained from weather stations at Auckland, Leigh, Mokohinau Islands, Onehunga, Paeroa, Whangaparoa and Whangarei. Duplicate data were removed and gaps were filled using linear interpolation (largest gap was 6 hrs). Data from the seven stations were interpolated over the Hauraki Gulf grid area using a cubed inverse-distance routine and the file then cropped to the Firth of Thames model region. The default wind friction coefficient was used for the simulations.

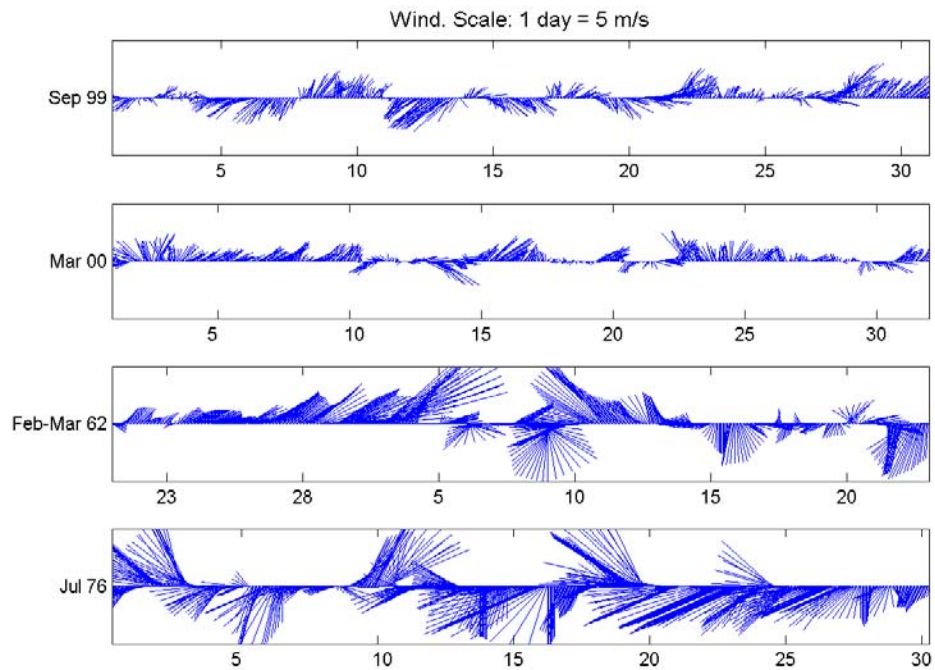
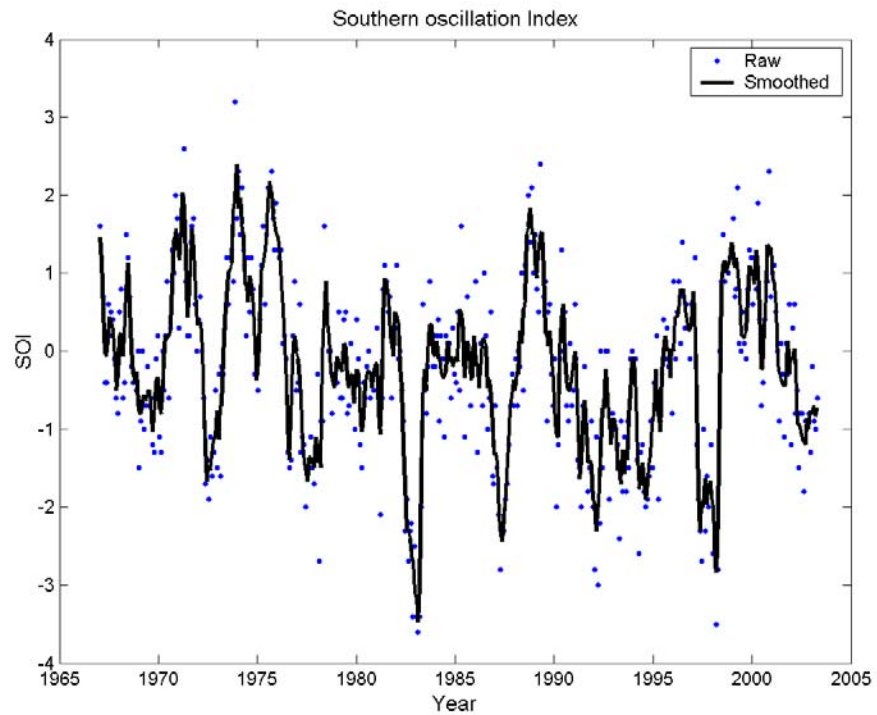


**Figure 4:** Wind used in numerical simulations. Data is plotted in meteorological convention (feathers project in the direction from which the wind blows). The upper two plots show winds from the calibration simulations, the 1962 data was used in simulations of “worst-case” winds from ENE, and 1976 data was used in “worst-case” WSW simulations.

Winds used to force the calibration simulations are shown in Figure 4, the September 1999 period was characterised by relatively higher occurrence of southwesterly winds, compared with the March 2000 period, which contained more northeasterly winds. The calibration periods therefore contain typical seasonal differences, southwesterlies being common in winter and northeasterlies in summer, explained further below.

### 2.3.6 “Worst-case” winds

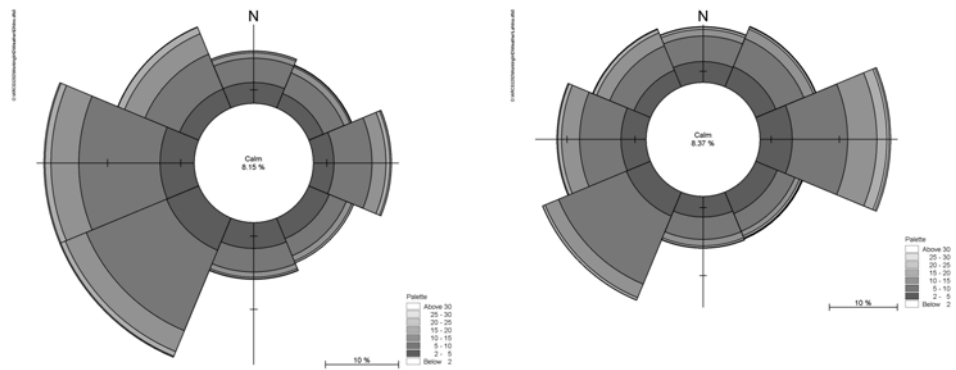
One of the modelling objectives was to simulate conditions representative of “worst-case” scenarios that might present themselves during El Nino or La Nina conditions. The Mokohinau Island wind record was examined, because it is a long-term record and is a coastal wind station that is less likely to suffer topographic interference than stations on the mainland. 115,367 wind readings were available for the period 1961–2000 although there was a 10-year gap in the record 1984–1994. The monthly SOI was running-averaged using a 3-month window, and La Nina and El Nino periods were selected where the SOI exceeded a value of 1 and -1 respectively (Figure 5).



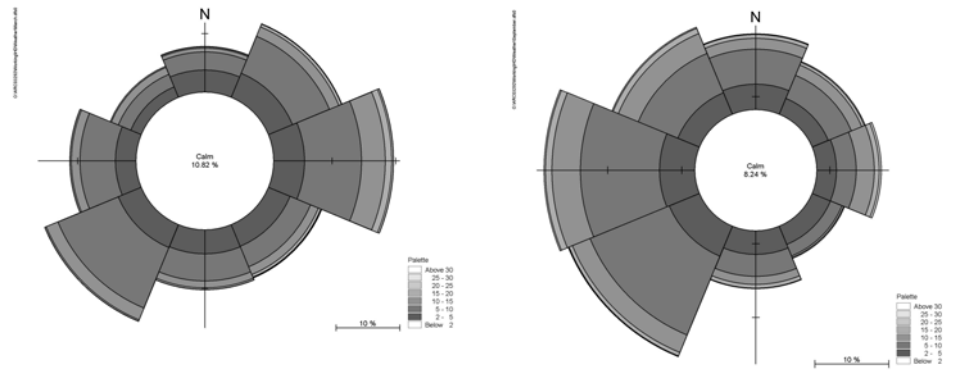
**Figure 5:** Southern oscillation index, 1967–2003.

Figure 6 shows wind roses for El Nino and La Nina periods, it is seen that winds blowing from the W and SW are more prevalent during El Nino years and winds blowing from the E and NE are more prevalent during La Nina years.

Figure 7 shows wind roses for the months of March and September. These wind roses are similar in form to seasonal wind roses for summer–autumn and winter–spring respectively. Comparing Figure 6 and 7, it can be seen that the September (Winter) wind rose is similar to the El Nino rose, while the March (Summer) rose is similar to La Nina.



**Figure 6:** Wind roses for El Nino (left) and La Nina (right) periods, from 21,368 and 21,183 readings respectively of a total 115,367 readings (each sector projects in the direction from which the wind blows).



**Figure 7:** Wind roses for March (left) and September (right) months, from 10,160 and 9,259 readings respectively of a total 115,367 readings (each sector projects in the direction from which the wind blows).

The seasonal effect shown in 7 masks the SOI signal, which makes it impossible to choose any 1-month (simulation length) wind record to represent SOI effects. For example, even though La Nina years have more easterly winds when averaged over the *whole year*, we don't necessarily see more easterly winds in September during La Nina years than we do in September during El Nino years. Therefore, I could not achieve the initial objective of simulating a 1-month period that is representative of either El Nino or La Nina *wind* conditions.

Instead I elected to find periods when the wind met certain criteria, based on the broad pattern of more northeasterlies in La Nina and southwesterlies in El Nino. Using a sliding 30-day window, periods were selected where the wind approached from either the NE-N or

SW–W sectors for more than 50% of the time. For each sector, the selected periods were then ranked on their closeness of fit to a wind speed criterion, the mean NE–E wind speed should be 2 standard-deviations above the long-term NE–E mean, while the SW–W speed should be 2 standard-deviations below, and vice versa. The closest matches were found and the wind roses were checked to ensure a reasonable wind speed distribution between fast and slow winds. The period 21 Feb to 23 March 1962 was chosen to represent winds prevailing from the ENE, and the period 30 June to 30 July 1976 to represent winds prevailing from the WSW (Figure 4, Figure 8). It is seen from Figure 4 that the chosen “worst-case” wind periods were considerably more energetic than the calibration periods, with relatively prolonged periods of uni-directional wind.

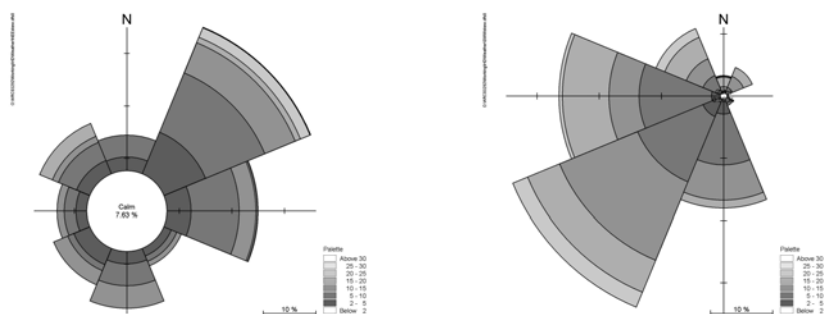


**Figure 8:** Wind roses of 30-day wind records used to represent “worst-case” NE and SW wind scenarios. (Each sector projects in the direction from which the wind blows).

### 2.3.7 Rivers

Monthly average river discharge information was obtained from 12 automatic flow gauging sites and supplemented for other major catchments surrounding the Firth of Thames using estimated runoff (Hadfield et al. 2002), and these were combined to give monthly average runoff at the river outlets marked in Figure 2. A 1-month lead in simulation was undertaken before each of the calibration simulations to allow river water to mix into the Firth of Thames to create more realistic initial conditions.

### 2.3.8 Heat exchange

Dry-bulb temperature readings from Auckland, Leigh, Mokohinau Islands and Paeroa were averaged to create a temperature timeseries for input to the model (Figure 9). Temperatures at the four sites showed generally close agreement, the sites are close together relative to the scale of weather systems that move across New Zealand.

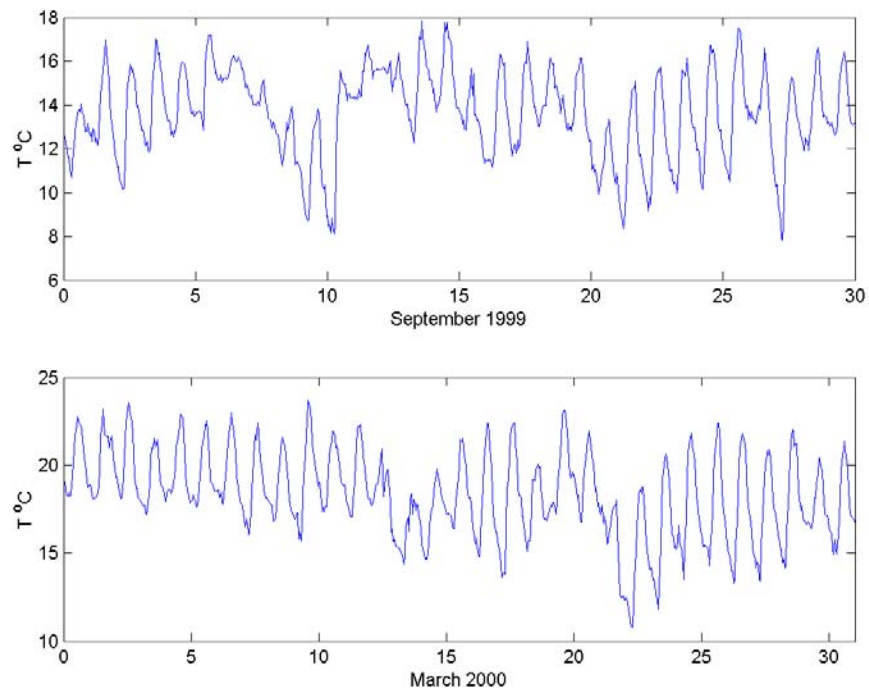


**Figure 9:** Air temperature timeseries used for model simulations.

### 2.3.9 Relative Humidity

Humidity is an important control on air-sea heat exchange. In the absence of sea-based measurements, relative humidity measurements from land-based weather stations were trialled, but these did not provide any better results than the default value of 88%, so relative humidity was set to 88% in the model.

### 2.3.10 Model output

Velocity in the horizontal and vertical directions, temperature and salinity were output at ½-hour intervals.

Whilst it is conceivable that large-scale farm development may modify flow patterns, I have not considered this. Initial studies have shown that currents do slow as they pass through marine farms, but the extent of retardation is not well known. Enhanced friction and slower flows will affect the amount of time that larvae are held inside the farm domain, and will therefore effect production estimates *inside* the farm area. The presence of farms is unlikely to greatly modify hydrodynamics in the Firth of Thames, and therefore should have only minor affect on larvae dispersal *outside* the farms.



## 3. Model calibration

### 3.1 Tides

The Nearshore-Offshore Exchange Programme produced a calibrated Hauraki Grid model for the twice-daily  $M_2$  lunar tides, based on boundary conditions from Proctor & Greig (1989). Since then Walters et al. (2001) have established a finite-element model of tides throughout the New Zealand Economic Exclusion Zone (EEZ). With this new model, earlier boundary conditions could be refined and extended to obtain a good calibration across the whole Hauraki model grid for tidal constituents  $M_2$ ,  $S_2$ ,  $N_2$ ,  $K_2$  (the main twice-daily lunar and solar tides) and  $K_1$ ,  $O_1$ ,  $P_1$  and  $Q_1$  (smaller once-daily lunar and solar tides), using model 3dd (Black 1995).

For this study a calibration for the  $M_2$  tidal component was undertaken over the Hauraki Gulf using MIKE3, with calibration results showing good agreement to measurements (Table 1 and Table 2), and similar phase and amplitude to the original model 3dd calibration results.

**Table 1:** Calibration of the Hauraki Gulf MIKE3 model against  $M_2$  tidal height amplitudes (cm) and phases ( $^\circ$ , NZST) recorded at site positions shown in Figure 1.

$M_2$	Observed		Modelled		Observed-model	
	Amplitude	Phase	Amplitude	Phase	Amplitude	Phase
C1	89	209	83	201	6	8
C2	85	203	81	199	4	4
C3	86	199	86	198	0	1
C4	91	203	101	202	-10	1
C5	91	202	91	192	0	10
C6	103	208	101	199	2	9
C7	116	204	112	204	4	0
C8	102	198	110	201	-8	-3
C9	116	202	109	199	7	3
C10	101	206	113	202	-12	4
C11	127	204	123	200	4	4
C12	88	205	84	202	4	3
C13	88	206	83	201	5	5
C14	89	205	83	202	6	3
C15	90	204	84	201	6	3
C16	97	204	86	198	11	6

The tidal calibration results indicated that the 750 m bathymetry grid was adequate to accurately resolve tidal flows, and that the EEZ model was providing accurate tidal predictions to force the model.

**Table 2:** Calibration of the Hauraki Gulf model against  $M_2$  tidal velocity measurements from moored current-meters in ellipse form. Phases are for peak flow and in terms of NZST. Site positions shown in Figure 1.

$M_2$	Observed			Modelled			Observed-model		
	Major velocity	Inclination	Phase	Major velocity	Inclination	Phase	Major velocity	Inclination	Phase
T1	15	-17	288	16.9	86	296	-1.9	-103	-8
T2	18	7	298	16.4	70	296	1.6	-63	2
T3	19	-1	294	19.5	93	293	-0.5	-94	1
T4	19	2	285	18.9	85	283	0.1	-83	2
T5	19	0	284	19.1	84	284	-0.1	-84	0
T6	11	32	294	12.3	55	293	-1.3	-23	1
T7	13	8	285	15.5	84	292	-2.5	-76	-7
T8	49	74	303	48.2	11.4	299	0.8	62.6	4

### 3.2 Temperature calibration

Temperature calibration was hampered by lack of relative humidity, air temperature and water clarity data.

There are a number of complex coefficients in the heat exchange formulation of the model, reflecting the complexity associated with heat exchange between the ocean and atmosphere. The heat exchange with the atmosphere affects the water temperature and is very important to biological activity. It is calculated on basis of four physical processes: the long wave radiation, the sensible heat flux (convection), the short wave radiation, the latent heat flux (evaporation). There are coefficients for Daltons law controlling vaporative heat loss (or latent flux), for Angstroms law controlling daily radiation under cloudy skies, and light penetration and extinction coefficients.

These coefficients were experimented with, but in the end were left at default values because the most effective parameters at controlling heat exchange were the physical variables of air temperature and relative humidity, and these factors themselves were not well known. For example, relative humidity was unknown and was left at the default value of 88%, and air temperature was only available for land-based stations.

Stratification was initially found to break down rapidly in the model as heat was being dispersed too rapidly into deeper layers. This problem was solved by reducing the vertical temperature dispersion factor by a factor of ten, from the default value 0.1 to 0.01, which kept the heat in the surface layers.

In the end, adequate temperature calibration was obtained for March 2000 by using the temperature timeseries shown in Figure 9, and adding 3°C. For the September 1999 simulation, a constant air temperature of 16°C was substituted for the land-based measured temperature timeseries shown in Figure 9.

During the March 2000 calibration the model reproduces the basic temperature structure at the mooring site (Figure 10). The modelled thermocline level is close to that measured, but is about 2 m shallower. The heat pulse in the surface water on days 7 to 14 and subsequent cooling is reproduced with a lag of about 1-day in the model.

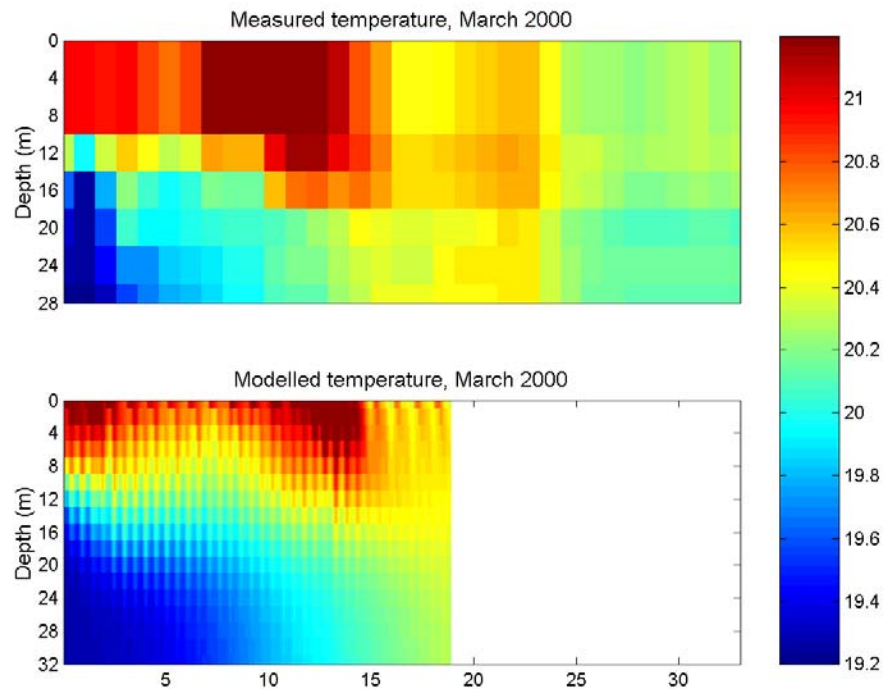


**Figure 10:** Comparison between measured (upper) and modelled (lower) temperatures at the long-term mooring site (Figure 2) during March 2000. Measurements have been interpolated to 4 m intervals, and those above 10 m have been set equal to the uppermost available thermistor measurement. This is justified by Figure 11, which shows the upper water column to be thermally well mixed.

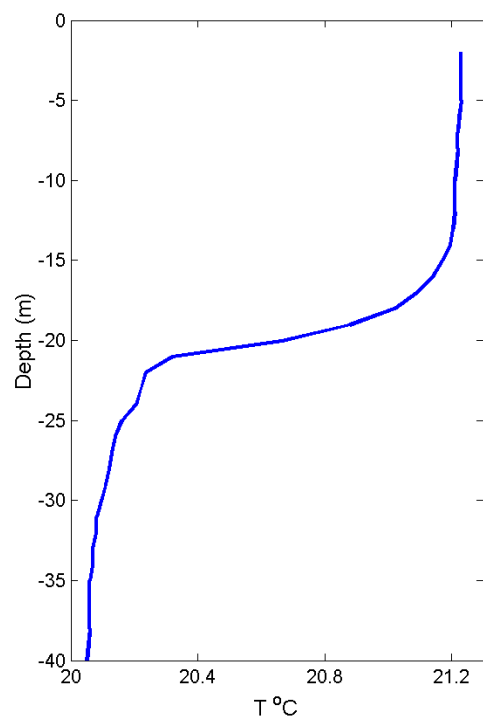


**Figure 11:** Temperature profile from a CTD cast taken at the mooring site (Figure 2), during a one-day sampling cruise (10:10, 10 March 2000).

During the September 1999 calibration the model also reproduces the basic temperature structure with reasonable success (Figure 12).

The temperature calibrations are an encouraging result, considering the complexities of thermal heat transport.

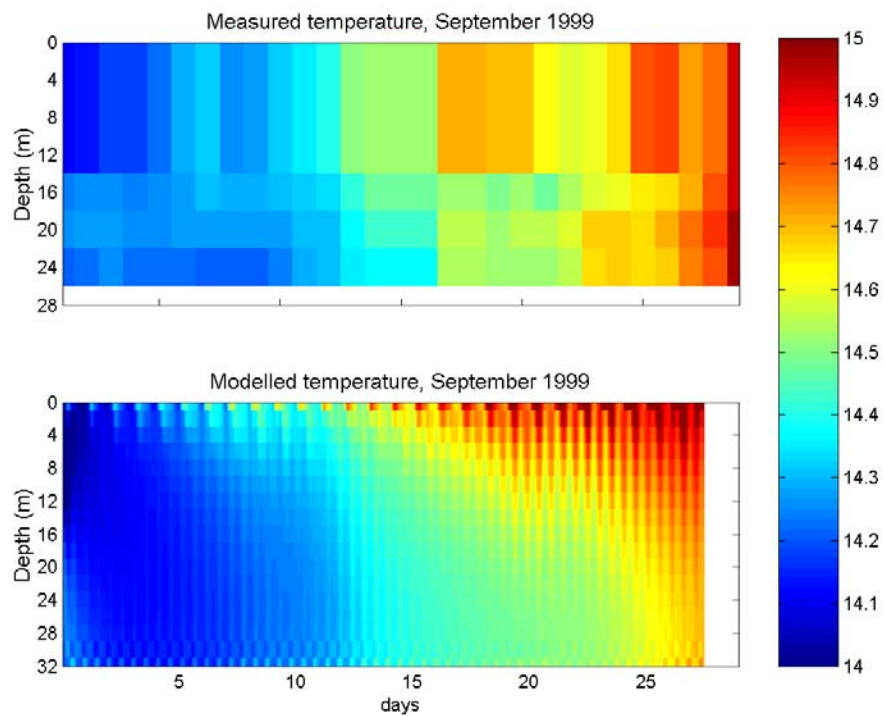


**Figure 12:** Comparison between measured (upper) and modelled (lower) temperatures at the long-term mooring site (Figure 2) during September 1999. Measurements have been interpolated to 4 m intervals, and those above 10 m have been set equal to the uppermost available thermistor measurement.

### 3.3 Residual currents

In Figure 13 a current-meter record from late summer 2001 is compared with the calibration simulation. Unfortunately there were no corresponding time-periods to compare, but the directional trend and the migration rates are similar between the two time periods. All the current-meter records (both summer and winter) from this site showed similar long-term trends, currents flowing southward towards the Firth of Thames near the seabed. This agrees with simulated time-averaged flow (e.g., Figure 15, Figure 17).

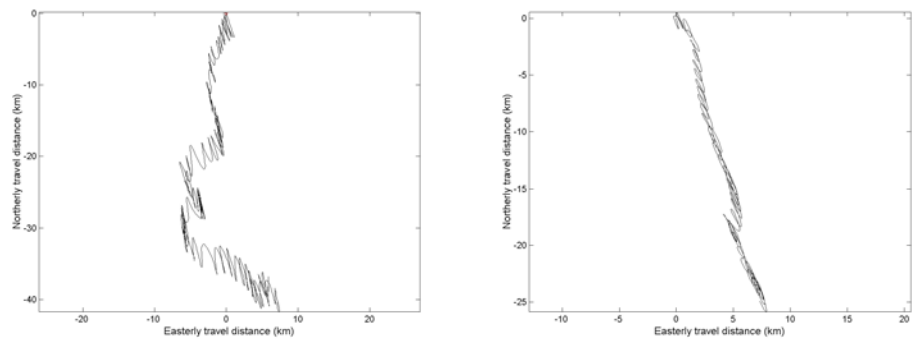


**Figure 13:** Cumulative vector plots. On the left – from an Aanderaa current-meter deployed at the mooring site (Figure 2) from 15 March – 15 April 2001, 9 m above the seabed. On the right – from the March 2000 calibration simulation at a corresponding position; model cell 81,71, layer 28–30 m below the surface.

## 4. Results – Firth of Thames hydrodynamics

Currents in the Firth of Thames are forced primarily by tides, winds and river flows, in that order of importance. Solar and freshwater inputs add structure by stratifying the water column.

### 4.1 Tidal currents

Tidal flows are strongest in the outer Firth (Figure 14), reaching  $0.4 \text{ m s}^{-1}$  during spring tides. Neap tidal currents are reach about  $0.2 \text{ m s}^{-1}$ . Tidal currents accelerate past Deadmans Point near Kirita Bay. Tidal currents are less than  $0.05 \text{ m s}^{-1}$  in the shallow southern Firth.

Time-average currents (sometimes called residual currents) show long-term water migration trends and indicate cumulative flow features. For example, they may indicate a tendency for currents to flow through a marine farm area when averaged over a long time period. The time-averaged plots shown below have all been averaged to the nearest complete tidal cycle over the entire simulation period, being one month in most cases.

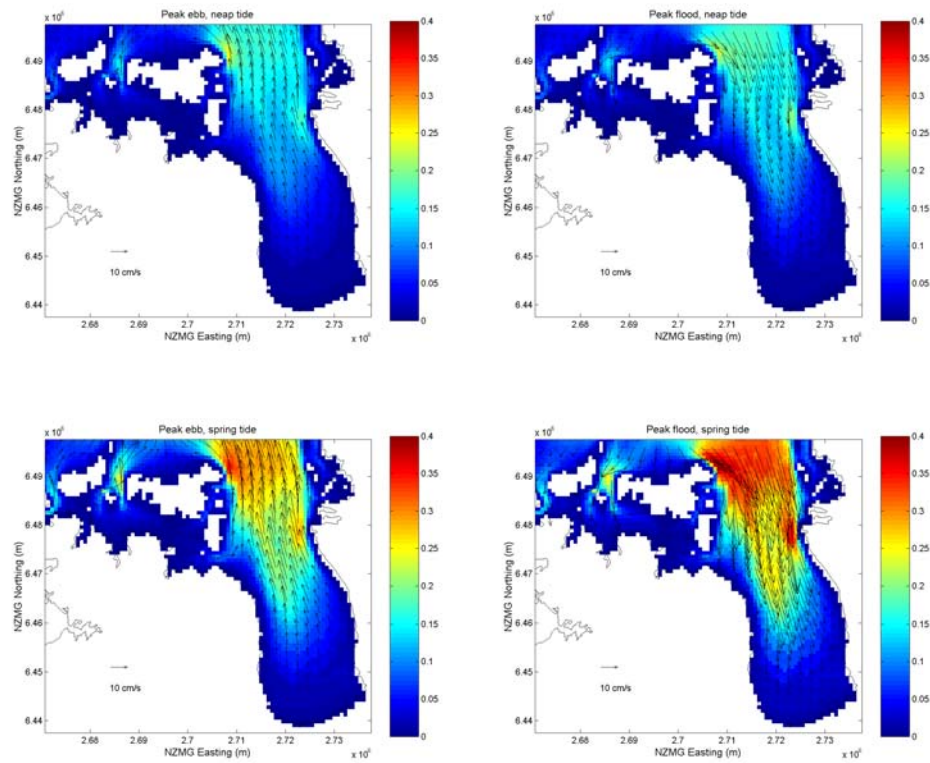


**Figure 14:** Peak instantaneous depth-averaged tidal currents, neap (2 March 2000) and spring (22 March 2000). Colour-scale represents  $\text{m s}^{-1}$ .

To assess the time-averaged tidal flow, Figure 15 shows time-average currents for March 2000, using tides and temperature inputs, but no wind or river inflows. Tidal currents tend to flow southward into the Firth of Thames below 10 m depth and northward out of the Firth of Thames at the surface. The Earth's rotation gives rise to the Coriolis force, which causes currents to be deflected to the left in the Southern Hemisphere. The time-averaged surface flow out of the Firth is therefore deflected to the left, and flows strongest past Ponui and Waiheke Islands. This is balanced by a tendency for deeper currents flowing southward into the Firth to be deflected towards the Coromandel peninsula. The flooding tide also gets squeezed around Waiheke Island as it enters the Firth from the Hauraki Gulf, therefore the flood tide is stronger than the ebb tide near Kirita Bay, and the strong flood currents are deflected upward and westward by Deadmans Point. This forces time-averaged upwelling and surface flow offshore towards the west in the vicinity of Wilson's Bay. The above tidal flow description applies equally well to the September 1999 winter simulation, because stratification does not greatly affect the tidal wave.



**Figure 15:** Simulated time-average currents during March 2000, using tides and temperature inputs, but no wind or river inflows. Plots are for horizontal layers, from upper right to lower left: 0-2 m, 8-10 m, 18-20 m, 28-30 m below mean sea level.

## 4.2 Wind-driven currents

Wind stress adds to and modifies the tidal flows. The instantaneous currents are generally dominated by tides, but the cumulative wind-driven affect can be seen in the time-averaged flow. Figure 16 shows currents during strong west-southwest winds; they are averaged over a tidal cycle and are mostly wind-generated. In the stratified summer simulation (plots on the left), the surface currents were pushed northward, with a slow return flow down the centre of the Firth. The currents were more spatially uniform and generally faster than in the unstratified winter simulation (on the right). In the winter, an anticlockwise eddy was

generated in the Firth that extends from the surface to the seabed and current jets were evident in the Hauraki Gulf.

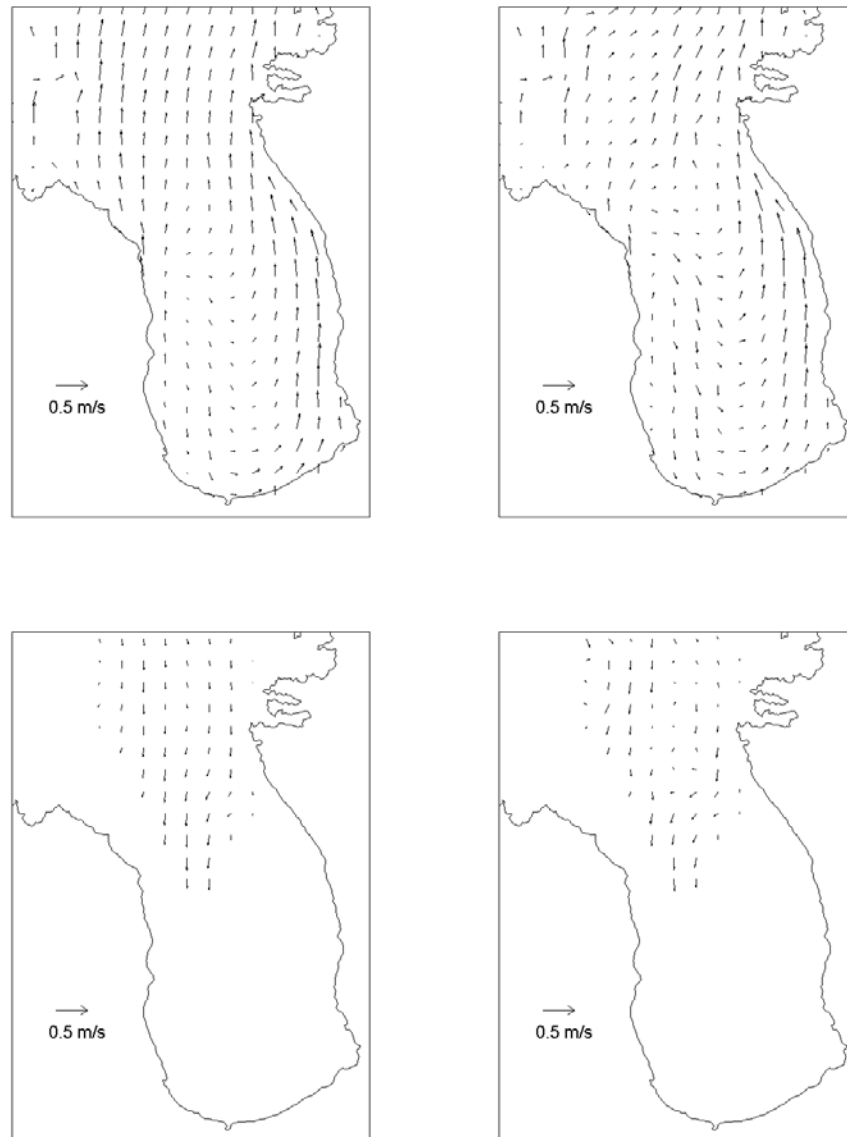


**Figure 16:** Simulated currents, time-averaged over 1 tidal-cycle during strong WSW winds (wind conditions from 6 July 1976, Figure 4). Plots on the left correspond to hydrodynamic conditions 6 March 2000 (summer) and those on the right to hydrodynamic conditions from 6 September 1999 (winter). Upper plots are 0-2 m, while lower are for 18-20 m below the water surface.

For example, during the calibrated March 2000 simulation (Figure 17) the wind helped push stronger surface currents out of the Firth and draw bottom currents faster than would have occurred during calm conditions (Figure 15). River flows also contributed to push surface currents out of the Firth, but their contribution was minor in comparison to tide and wind.

Variable winds in the absence of stratification contributed to high variability of time-averaged currents during September 1999 (Figure 18).

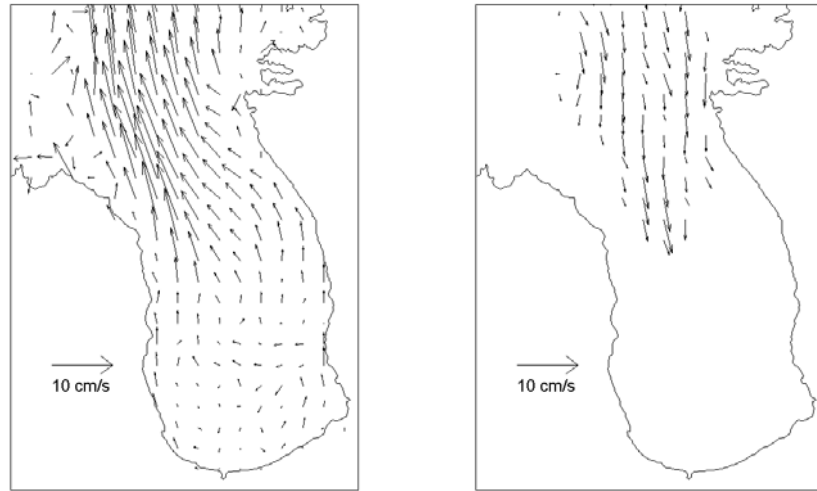


**Figure 17:** Time-average currents during the March 2000 calibration simulation, using tide, wind, river and temperature inputs. Plots are for horizontal layers, 0-2 m and 18-20 m below mean sea level.

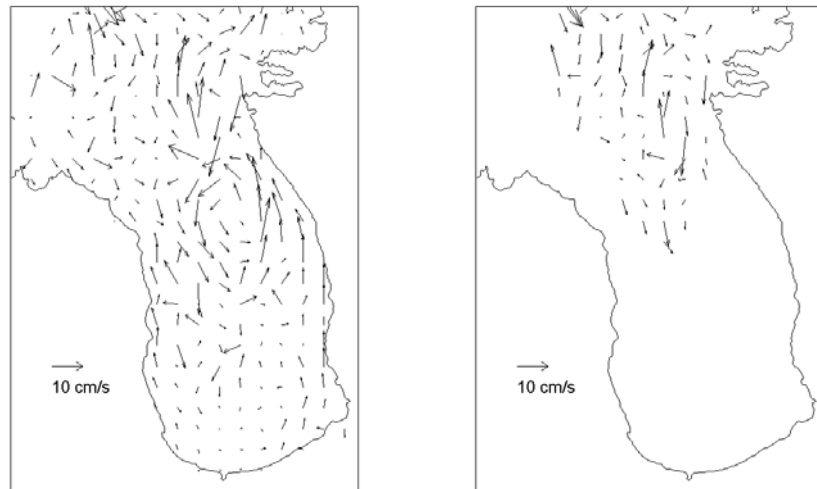


**Figure 18:** Time-average currents during the September 1999 calibration simulation, using tide, wind, river and temperature inputs. Plots are for horizontal layers, 0-2 m and 18-20 m below mean sea level.

### 4.3 “Worst-case” winds

Figure 19 to Figure 22 show time-average currents near the surface and at 18-20 m depth, for summer and winter simulations using “worst-case” ENE and WSW winds (Figure 4).

During summer, stratification allowed surface wind-driven flows to easily shear across deeper currents, with return flows occurring underneath. During the ENE wind simulation, surface currents were pushed southwest with a time-averaged clockwise circulation in the lower Firth, and deep currents returned toward the north (Figure 19). During the WSW wind simulation, surface currents were pushed northeast with a time-averaged anticlockwise circulation in the lower Firth, and deep currents returned toward the southwest (Figure 20). The affect of stratification in de-coupling vertical water “layers” means that particles near the water surface are likely to remain there and be transported faster by wind-driven flows during summer than in winter.

During winter the water column was not strongly stratified. This meant that wind-driven currents were not confined to the upper water column and return-flows were less likely to form underneath. Instead of downwelling at the down-wind coast, wind-driven currents were more inclined to bend around, steered by the bathymetry. During winter therefore, currents were less likely to flow uniformly in the wind direction (at the surface) and displayed higher horizontal variability. As a result the time-averaged plots during winter are a complex accumulation of horizontally variable flow. Despite this extra horizontal variability, the winter “worst-case” simulations (Figure 21, Figure 22) still show the same basic trends as occurred during the summer simulations.

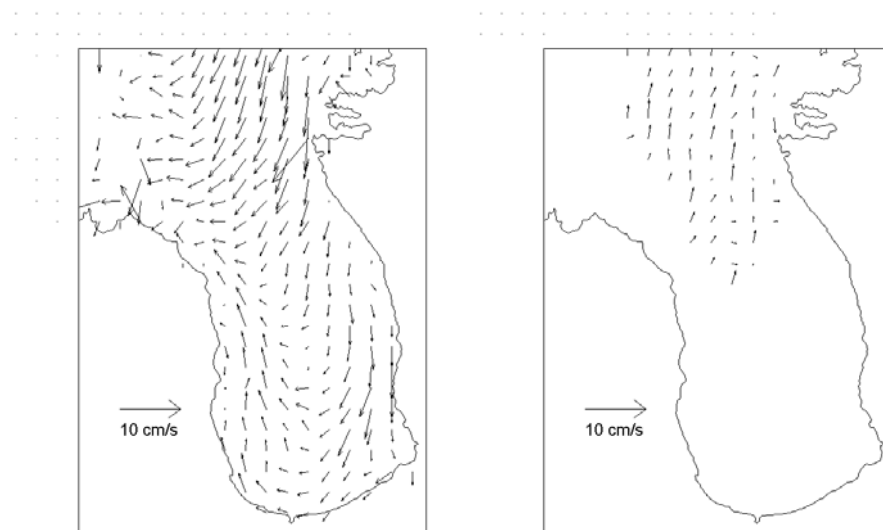


**Figure 19:** Time-average currents using tide, ENE “worst-case” winds, river and temperature. Temperature inputs were those of March 2000. Plots are for horizontal layers, 0-2 m and 18-20 m below mean sea level.

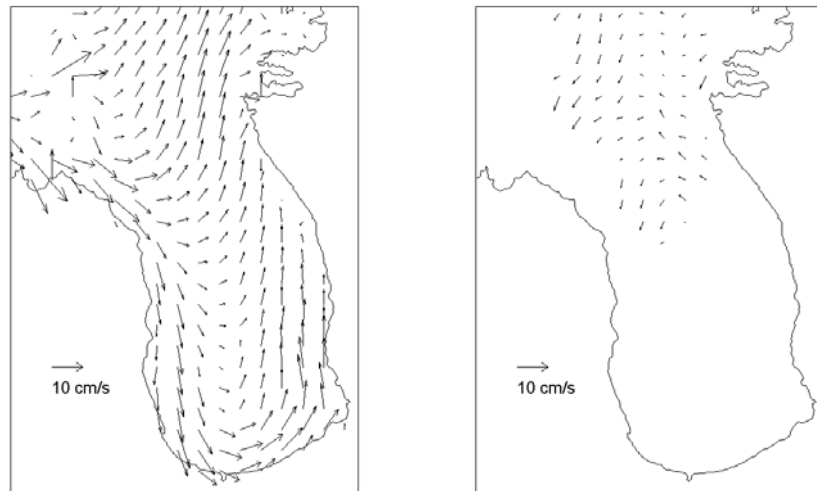


**Figure 20:** Time-average currents using tide, WSW “worst-case” winds, river and temperature. Temperature inputs were those of March 2000. Plots are for horizontal layers, 0-2 m and 18-20 m below mean sea level.

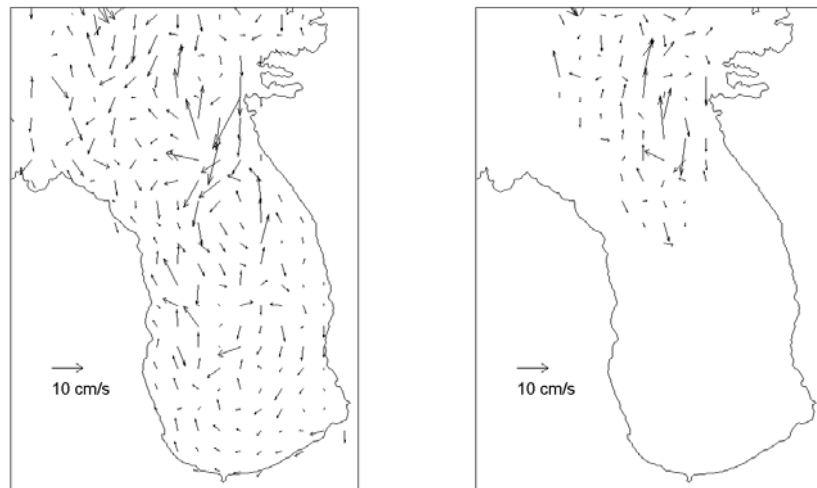


**Figure 21:** Time-average currents using tide, ENE “worst-case” winds, river and temperature. Temperature inputs were those of September 1999. Plots are for horizontal layers, 0-2 m and 18-20 m below mean sea level.

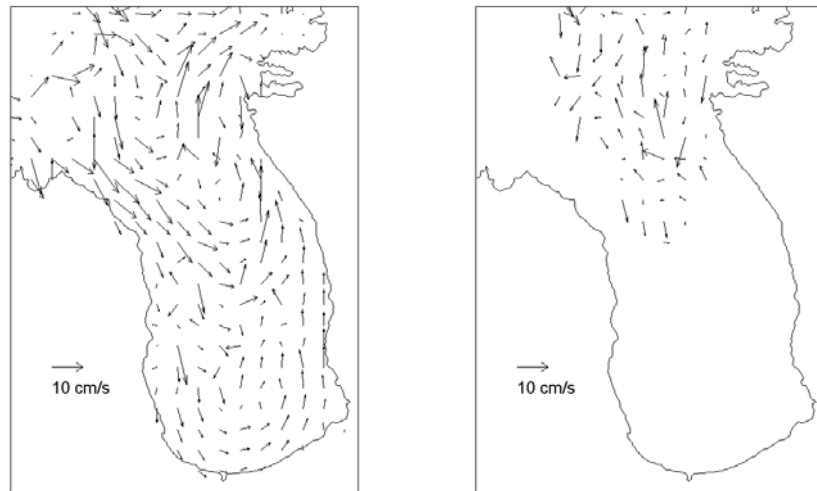


**Figure 22:** Time-average currents using tide, WSW “worst-case” winds, river and temperature. Temperature inputs were those of September 1999. Plots are for horizontal layers, 0-2 m and 18-20 m below mean sea level.

## 5. Conclusions

Tides dominate the instantaneous flow field in the Firth of Thames, with strongest flows in the outer Firth reaching 0.2 and 0.4 m s<sup>-1</sup> during neap and spring tides respectively. Tidal flows are less than 0.05 m s<sup>-1</sup> in the shallow southern Firth. Flood tides are deflected upward around Deadmans Point, causing time-averaged upwelling in its vicinity.

The Earth's rotation deflects currents to the left, causing flood tides to be stronger on the eastern side near Wilsons Bay and ebb tides to be stronger on the western side.

Wind is of secondary importance to the instantaneous currents, but has a dominant influence on time-averaged currents, which show cumulative flow features. When winds approach from the ENE, surface currents are pushed southwest with a time-averaged clockwise circulation in the lower Firth, and deep currents returned toward the north. When winds approach from the WSW, surface currents are pushed northeast with a time-averaged anticlockwise circulation in the lower Firth, and deep currents returned toward the southwest.

The affect of stratification in de-coupling the water column means that particles near the water surface are likely to remain there and be transported faster by wind-driven flows during summer than in winter.



## 6. References

- Black, K.P. (1995). The hydrodynamic model 3DD and support software. *Occasional Report No. 19*. The University of Waikato. 53 p.
- Black, K.P.; Bell, R.G.; Oldman, J.W.; Carter, G.S.; Hume, T.M. (2000). Features of 3-dimensional barotropic and baroclinic circulation in the Hauraki Gulf, New Zealand. *New Zealand Journal of Marine and Freshwater Research 34*: 1-28.
- Goring, D.G. (2001). Computer models define tidal variability. *American Institute of Physics 7(5)*.
- Hadfield, M.; Uddstrom, M.; Goring, D.; Gorman, R.; Wild, M.; Stephens, S.; Shankar, U.; Niven, K.; Snelder, T. (2002). Physical variables for the New Zealand Marine Environment Classification System: development and description of data layers. *No. CHC2002-043*, 59 p.
- Proctor, R.; Greig, M.J.N. (1989). A numerical model investigation of the residual circulation in the Hauraki Gulf, New Zealand. *New Zealand Journal of Marine and Freshwater Research 23*: 421-442.
- Walters, R.A.; Goring, D.G.; Bell, R.G. (2001). Ocean tides around New Zealand. *New Zealand Journal of Marine and Freshwater Research 35*: 567-579.



## 7. Glossary

Bathymetry	Underwater topography, a term often used to describe its representation in a numerical model grid.
Downwelling	Shallow water sinking toward the seabed.
Hydrodynamic	Water movement.
Stratification	Separation of a water column into horizontal layers by density — less dense (i.e., warmer, fresh) water on top.
Thermocline	The boundary zone or temperature gradient between the two layers in a thermally stratified water column.
Upwelling	Deep water rising toward the surface.